1120
doi:10.1017/S143192762200472X
Microsc. Microanal. 28 (Suppl 1), 2022

Elucidating the 3D Structure of β-(1,3)-glucan Synthase from *Candida glabrata* by Subtomogram Averaging

Jennifer Jiang[1,2], Cristina Jiménez-Ortigosa[3], Muyuan Chen[4], Kelley R. Healey[5], Joyce Kong[6], Yun-Kyung Lee[1,2], Daniel P. Farrell[7,8], Frank DiMaio[7,8], David S. Perlin[3], Wei Dai[2,1*]

[1.] Institute for Quantitative Biomedicine, Rutgers, The State University of New Jersey, Piscataway, NJ, United States
[2.] Department of Cell Biology and Neuroscience, School of Arts and Sciences, Rutgers, The State University of New Jersey, Piscataway, NJ, United States
[3.] Hackensack Meridian Health-Center for Discovery and Innovation, Nutley, NJ, United States
[4.] SLAC National Accelerator Laboratory, Stanford University, Menlo Park, CA, United States
[5.] Department of Biology, William Paterson University, Wayne, NJ, United States
[6.] Ernest Mario School of Pharmacy, Rutgers, The State University of New Jersey, Piscataway, NJ, United States
[7.] Department of Biochemistry, University of Washington, Seattle, WA, United States; Institute for Protein Design, University of Washington, Seattle, WA, United States
[8.] Institute for Protein Design, University of Washington, Seattle, WA, United States
* Corresponding author: wd157@dls.rutgers.edu

Invasive mycoses are emerging as a serious public health problem. The opportunistic fungal pathogen, *Candida glabrata*, is a leading cause of fungal infections in clinical settings due to its intrinsic low susceptibility and acquired resistance to widely used azoles [1]. Echinocandin antifungals have become the preferred front-line therapy to treat invasive candidiasis. Echinocandins inhibit fungal cell wall biosynthesis by targeting the catalytic subunit of the membrane-embedded enzyme complex β-(1,3)-glucan synthase (GS), resulting in osmotic instability and cell death [2]. Increasing clinical use of echinocandins has led to resistance, which is attributed to well-defined amino acid substitutions in highly conserved hotspot regions of the catalytic subunits of GS [3]. However, the location of the echinocandin binding pocket and the molecular mechanisms of drug action have not been defined due to the lack of three-dimensional (3D) structures of GS complexes. A major challenge lies in the purification of such a large membrane protein complex for structure characterization studies by X-ray crystallography or single particle analysis.

To address the technical challenges in purification of GS, we performed cryo-electron tomography (cryoET) on isolated plasma membranes from *C. glabrata* cells and subtomogram averaging to resolve the 3D organization of GS [4]. We constructed strains that overexpress the constitutive *FKS1* gene to enrich GS complexes in plasma membranes (Fig. 1A). From tomograms of plasma membranes extracted from Fks1-overexpressing cells (KH238 strain), we observed that GS complexes form tightly packed clusters that are heterogeneously distributed on large membrane regions (Fig. 1B).

To investigate the domain organization of the GS complexes, we performed subtomogram averaging with particles extracted from plasma membrane tomograms. The subtomogram average of GS clearly showed extra-membrane domains protruding towards one side of the membrane. A topological model of Fks1 from *Saccharomyces cerevisiae* reported localization of the central catalytic domain to the cytosolic face of the membrane, consistent with our subtomogram average [5]. Within a Fks1 subunit, we also observed a potential channel extending from the cytosolic domain to the exoplasmic face of the

membrane. This channel may accommodate growing glucan chains and provide a route for their extrusion into the cell wall (Fig. 2A).

To better understand the structure of GS and its interaction with echinocandin drugs, we applied Rosetta-based structure prediction using the primary sequence of the *FKS1* gene from *C. glabrata* to generate *de novo* models of GS [6]. The model shows that secondary elements, particularly the transmembrane α-helices, were accurately delineated. Interestingly, mutations associated with echinocandin resistance localized to the exoplasmic side of the potential extrusion channel (Fig. 2C, left). Based on insights from both our subtomogram average and structural model of GS, binding of echinocandin likely inhibits GS by directly blocking the exit of glucan products through the extrusion channel. We also compared the Rosetta model to the AlphaFold model of GS from *S. cerevisiae* (Fig. 2C, right) [7]. The two models are relatively similar in terms of secondary structural arrangements and the location of resistance-conferring residues.

Structure determination of large macromolecular assemblies often requires a combination of experimental techniques to provide meaningful insights into the molecular mechanisms underlying their biological activities. Currently, different integrative modeling strategies can be used to assemble multi-domain protein structures under the constraints of medium-to-low resolution cryoEM density maps [8-9]. We aim to take advantage of this approach to build atomic models that provide biological insights into GS interaction with echinocandins. While protein structure prediction has become pivotal for structure-based drug discovery, higher resolution 3D maps of GS from experimental techniques remain a critical piece of the puzzle to validate structure prediction models and determine the molecular mechanisms underlying echinocandin inhibition of GS and antifungal resistance.

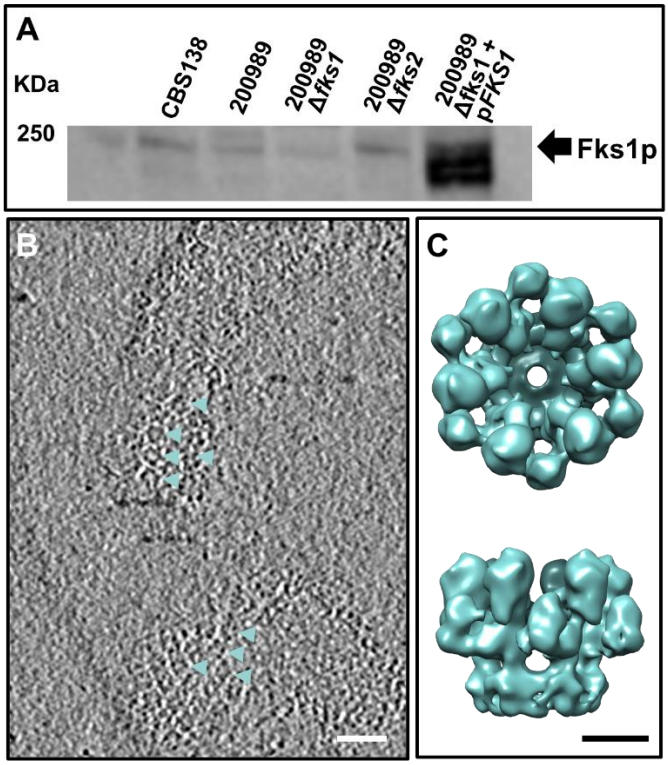

Figure 1. Cryo-electron tomography (cryoET) revealed ring-like structures in plasma membranes of *Candida glabrata* cells overexpressing Fks1. (A) Expression levels of Fks1. *C. glabrata* cells from

https://doi.org/10.1017/S143192762200472X Published online by Cambridge University Press

the different strains were grown on liquid YDP with (plasmid-carrying strains) or without 100 µg/mL nourseothricin until mid-log phase. Proteins were extracted using the TCA method. p*FKS1* = pCN-PDC-*FKS1*. (B) Slice view of a representative tomogram showing a cluster of ring-like structures from the Fks1-overexpressing (KH238) strain (teal arrows). (C) Isosurface, top (top) and side (bottom) views of the GS structure from KH238 plasma membranes. Scale bars = 5 nm.

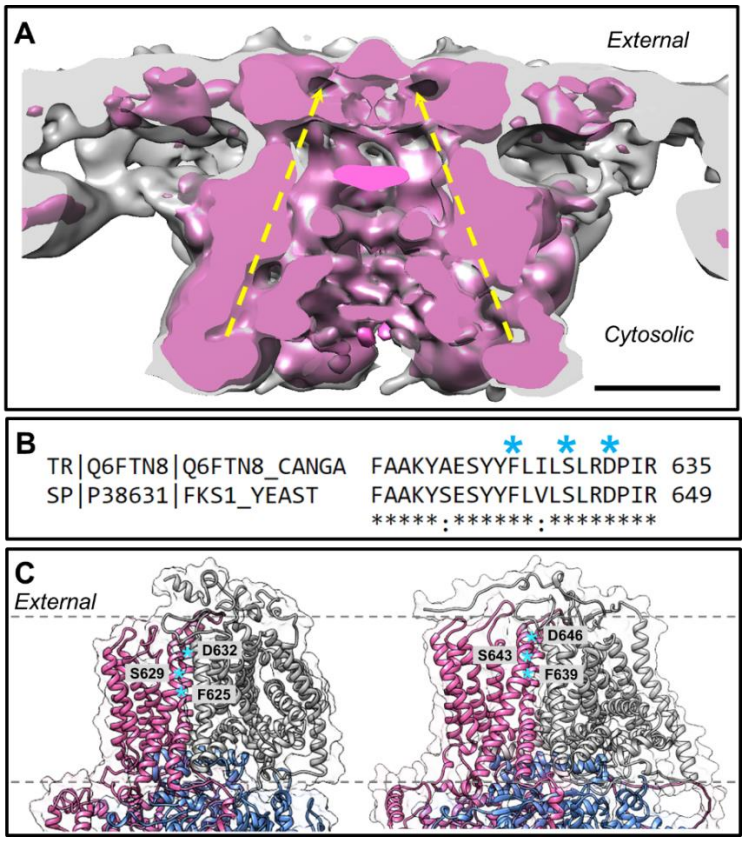

Figure 2. Subtomogram average and structure prediction models of GS reveal the location of amino acids associated with echinocandin resistance. (A) A cutaway view of the GS subtomogram average (pink, higher threshold; gray, lower threshold showing membrane density) with yellow dashed lines indicating potential extrusion channels for glucan products. Scale bar = 5 nm. (B) Homology alignment between *C. glabrata* (top) and *S. cerevisiae* (bottom) at the hotspot 1 region. Blue asterisks denote positions of resistance-conferring mutations in *C. glabrata* Fks1. (C) Ribbon representation of *C. glabrata* Fks1 from Rosetta-based structure prediction (left) and AlphaFold model of Fks1 from *S. cerevisiae* (right) showing the N-terminal (pink), central catalytic (blue), and C-terminal (gray) domains. Mutations in the hotspot 1 region are highlighted.

References

[1] Pappas, P.G., *et al.*, Nat Rev Dis Primers **4**, 18026 (2018). doi: 10.1038/nrdp.2018.26
[2] Douglas, C.M., Fungal β(1,3)-D-glucan synthesis **39**, 1 (2001), p. 55-66. doi: 10.1080/mmy.39.1.55.66
[3] Perlin, D.S., Clin. Infect Dis **61**, suppl_6 (2015), p. S612-S617. doi: 10.1093/cid/civ791
[4] Jiménez-Ortigosa, C., *et al.*, J Fungi **7**, 2 (2021), p. 1-13. doi: 10.3390/jof7020120
[5] Johnson, M.E. and Edlind, T.D., Eukaryot Cell **11**, 7 (2012), p. 952-960. doi: 10.1128/EC.00082-12

https://doi.org/10.1017/S143192762200472X Published online by Cambridge University Press

[6] Baek, M., *et al*., Science **373**, 6557 (2021), p. 871-876. doi: 10.1126/science.abj8754
[7] Jumper J., *et al.*, Nature **596** (2021), p. 583-589. doi: 10.1038/s41586-021-03819-2
[8] Farrell, D.P.., *et al*., IUCrJ **7**, Pt. 5 (2020), p. 881-892. doi: 10.1107/S2052252520009306
[9] Zhou, X., *et al.*, bioRxiv (2020). doi: 10.1101/2020.10.15.340455
[10] Tomographic data collected at Purdue University was supported by the National Institutes of Health Midwest Consortium for High Resolution Cryo-electron Microscopy (U24 GM116789-01A1). This work was supported by the National Institutes of Health (R01AI109025) to D.S.P. The authors acknowledge Jason T. Kaelber and Emre Firlar at the Rutgers CryoEM & Nanoimaging Facility for their support in data collection.